

IFSCC 2025 full paper (IFSCC2025-763)

Deciphering the Water-Holding Capability of Multifunctional Amphiphilic Polymer Esters: Insights from In Vitro Experiments and In Silico Simulations

Yuko MAEMA ANDA^{1,2}, Naoko HANADA YAMAZAKI¹, Kai YOSHIOKA¹, Fan MENG², Toshinori SAIDA¹, Keiichi OYAMA¹, Noriyoshi ARAI²

¹ The Nissin OilliO Group, Ltd., Japan.

² Department of Mechanical Engineering, Keio University, Japan.

1. Introduction

Water-in-oil (W/O) emulsifiers are essential for enhancing the stability and functionality of formulations, particularly in the cosmetic, pharmaceutical, and food industries [1-5]. These emulsifiers provide desirable properties such as moisturization, smooth texture, and long-term stability by dispersing fine water droplets within oil phases [6, 7]. Among existing W/O emulsifiers, Polyglyceryl-2 Dipolyhydroxystearate [8-10] is widely used in cosmetics due to its natural origin and high safety profile.

In this study, a novel polymer, “Ester A,” was developed through precise regulation of the degree of polymerization of Polyglyceryl-2 Dipolyhydroxystearate. Ester A is characterized by its amphiphilic nature, high viscosity, strong water resistance, and notable water-holding capability. The present study focuses on the water-holding capability of Ester A. Although water-holding is generally associated with W/O emulsification, it is treated here as a distinct concept and has yet to be clearly defined. Moreover, previous studies on emulsification have primarily focused on low-molecular-weight surfactants [11, 12], while research on polymeric emulsifiers remains limited [13, 14]. We hypothesized that the degree of polymerization of polymer esters influences their water-holding capabilities. To test this hypothesis, we compared the water-holding properties of Ester A and Ester B, which is a low-polymerized ester. However, understanding the detailed molecular behavior at the microscopic level remains challenging using conventional experimental techniques alone. To address this limitation, we employed molecular simulations to complement experimental methods and elucidate the underlying mechanisms at the molecular level.

The objective of this study is to elucidate the mechanisms underlying water-holding capability from both macroscopic (*in vitro*) and microscopic (*in silico*) perspectives, thereby providing a foundation for the development of novel materials with superior moisturization performance.

2. Materials and Methods

2.1 Materials

Polyglyceryl-2 Dipolyhydroxystearate (Esters A and B) was synthesized from 12-hydroxystearic acid and diglycerin in the presence of a metal catalyst, with the reaction conducted at high temperature. The synthesis process involved several variables, including heating temperature, reaction time, and mixing ratio of 12-hydroxystearic acid to diglycerin.

2.2 Characterization of Esters

Esters A and B were characterized by high-performance liquid chromatography (HPLC) using the ACQUITY Advanced Polymer Chromatography System (Waters Corporation). Calibration curves were first established using 11 polystyrene standards with varying degrees of polymerization, correlating molecular weight with retention time (coefficient of determination > 0.999). Esters A and B were then analyzed under these conditions, and their weight-average molecular weight (M_w) and polydispersity index (PDI) were calculated from the calibration curves.

2.3 Interfacial Tension Measurement

Interfacial tension measurements were performed using the du Nouy ring method with the DY-500 instrument (Kyowa Interface Science Co., Ltd.).

2.4 Evaluation of Water-Holding Capability

Ten grams of ester was heated in a water bath at 40°C, then dispersed using a mixer (IKA Japan K.K.). Water was added incrementally in volumes of 0.02-0.03 mL. The endpoint was defined as the point at which the ester no longer holds additional water. Water-holding capability was calculated using Equation (1), and the maximum capability was determined at the endpoint.

$$\text{Water-holding capability (\%)} = (\text{amount of water held}) / (\text{amount of ester}) \times 100 \quad (1)$$

2.5 Preparation of Hydrates

The ester was heated in a water bath at 40°C and then dispersed using a mixer (PRIMIX Corporation). Water was added in a specified amount, followed by stirring at 1,500 rpm for 5 min. The resulting hydrates were subsequently degassed using a standard method.

2.6 Optical Microscopy

Hydrates were placed between glass plates and observed at a constant temperature of 25°C. Images were captured using the VHX-7000 system (KEYENCE Corporation).

2.7 Differential Scanning Calorimetry (DSC)

Differential scanning calorimetry (DSC) measurements were performed using the DSC 7000X instrument (Hitachi High-Tech Corporation). Samples were placed in aluminum pans and sealed tightly. DSC curves were recorded at a cooling rate of $1^{\circ}\text{C min}^{-1}$.

2.8 Small- and Wide-Angle X-ray Scattering (SWAXS)

Small- and wide-angle X-ray scattering (SWAXS) measurements were conducted using a SAXSess instrument (Anton Paar GmbH), equipped with a long, fine-focus sealed glass X-ray tube ($\text{Cu Ka}, \lambda = 0.1542 \text{ nm}$). The instrument operated at 40 kV and 50 mA. Samples were

irradiated for 1 min at 25°C and loaded into a cell fitted with a Kapton film window, specially designed for the SAXSess camera.

2.9 Time Domain Nuclear Magnetic Resonance (TD-NMR)

Time domain nuclear magnetic resonance (TD-NMR) measurements were conducted at 20 MHz using the minispec mq 20 (BRUKER Corporation), and the transverse relaxation time (T_2) was recorded.

2.10 Molecular Simulations

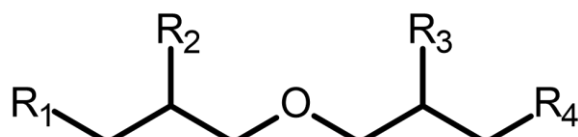
The dissipative particle dynamics (DPD) method [15-18], which enables simulations on millisecond timescales and micrometer length scales, was employed to track the motion of coarse-grained particles (each composed of groups of atoms or molecules). DPD is based on Newton's equations of motion. Each coarse-grained particle (bead) in the system was subjected to three types of intermolecular forces: conservative, dissipative, and random. To investigate the effect of polymerization degree on water-holding capability, simulations were performed on Esters A and B at 10% and 30% water content. The simulations were conducted in a cubic box with side lengths of $30 r_c$, containing 81,000 particles. This configuration allowed for precise observation and analysis of the dynamic behavior of Esters A and B under varying water content and polymerization degrees. The results of simulations using the DPD method are reported in reduced units. Each physical quantity was non-dimensionalized using the cutoff radius (r_c), particle mass (m), and energy ($k_B T$), where k_B and T represent the Boltzmann constant and temperature, respectively. In this study, r_c , m , and $k_B T$ were each set to 1.0 for consistency within the dimensionless formulation. The unit of time (t) was defined as:

$$t = (mr_c)^{1/2}/k_B T = 1.0.$$

3. Results

3.1 Synthesis of Esters with Different Degrees of Polymerization

Polyglyceryl-2 Dipolyhydroxystearate (Esters A and B) was synthesized (Figure 1) by adjusting the synthesis conditions. The physical properties of the polymer esters are summarized in Table 1. The weight-average molecular weight (M_w) of Ester A was 7,800, with a polydispersity index (PDI) of 1.45. In contrast, the M_w of Ester B was determined to be 4,100, with a PDI of 1.76. These results indicate that Polyglyceryl-2 Dipolyhydroxystearates with distinct degrees of polymerization were successfully synthesized. The fundamental physical properties of the two polymer esters were comprehensively evaluated. The interfacial tension between the polymer ester and water at 23.8°C was measured to be $10.0 \pm 0.3 \text{ mN} \cdot \text{m}^{-1}$ for Ester A and $6.1 \pm 0.1 \text{ mN} \cdot \text{m}^{-1}$ for Ester B, indicating that Ester B exhibited higher interfacial activity.



$R_1 - R_4$ = hydroxy group or poly(12-hydroxystearate).

Figure 1. Molecular structures of Esters A and B.

Table 1. Characterization of Polyglyceryl-2 Dipolyhydroxystearate. M_w represents the weight-average molecular weight, and PDI refers to the polydispersity index. The water-holding capability indicates the maximum amount of water an ester can hold, calculated using the formula: Water-holding capability = (Amount of water held) / (Amount of ester) × 100. The final column indicates the observed state of the hydrate when water was added beyond the maximum water-holding capability.

Esters	M_w	PDI	Interfacial tension between polymer ester and water / mN·m ⁻¹ (at 23.8°C)	Maximum water-holding capability %	States when excess Water was added to hydrates
A	7,800	1.45	10.0±0.3	434	Maintain the W/O type
B	4,100	1.76	6.1±0.1	152	Phase inversion to O/W type

3.2 Evaluation of Water-Holding Capability (Maximum Water-Holding Capability) of Polymer Esters

The water-holding capabilities of Esters A and B, which differ in their degrees of polymerization, were evaluated. The maximum water-holding capability was calculated using Equation (1). The results showed that Ester A achieved a value of 434%, whereas Ester B reached 152% (see Table 1). Notably, Ester A exhibited approximately three times the water-holding capability of Ester B. Furthermore, when the amount of water added exceeded the maximum water-holding capability, Ester A maintained its W/O-type structure, whereas Ester B transitioned to an O/W-type structure.

4. Discussion

4.1 Differences in Water-Holding States

The hypothesis that the degree of polymerization affects water-holding behavior and capability was tested using optical microscopy, DSC, TD-NMR, and SWAXS. Additionally, molecular-level behavior was investigated using DPD simulations.

Based on the findings in Section 3.2, which demonstrated differences in the water-holding capabilities of Esters A and B, we hypothesized that the states of their hydrates differ. Hydrates containing 10% and 30% water for Esters A and B were observed via optical microscopy (Figure 2, top). In the hydrate of Ester A, spherical water droplets were uniformly distributed, with average particle sizes of $3.0 \pm 2.9 \mu\text{m}$ (10% water) and $3.5 \pm 1.2 \mu\text{m}$ (30% water). In contrast, water droplets in the Ester B hydrate were mostly smaller than 1 μm and appeared to form clusters. These results confirm that the hydrate states differ between Esters A and B. Given that Ester B exhibited lower interfacial tension than Ester A (see Table 1), the smaller droplet size in the Ester B hydrate is likely due to its lower interfacial tension. DPD simulations (Figure 2, bottom) further supported this observation: water droplets were larger in Ester A than in Ester B.

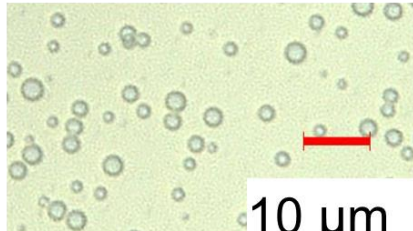
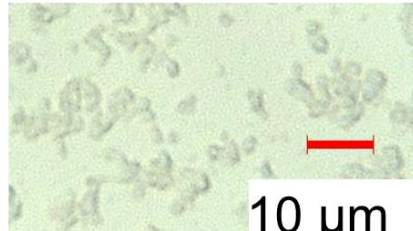
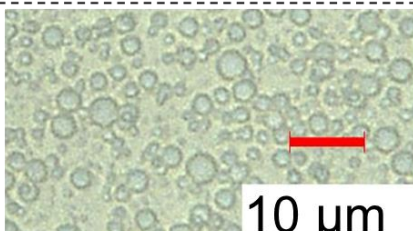
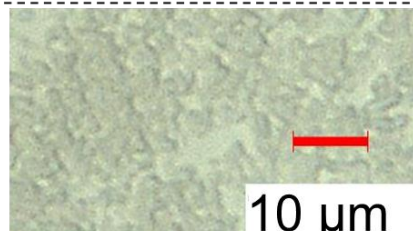
	Hydrate of A	Hydrate of B
Containing 10% water		
Containing 30% water		
Simulation snapshots of containing 30% water	 A 3D molecular simulation snapshot of a hexagonal prism containing a mixture of cyan and yellow spheres. The cyan spheres represent water molecules, and the yellow spheres represent polymer ester A molecules. They are distributed throughout the prism, with some clustering.	 A 3D molecular simulation snapshot of a hexagonal prism containing a mixture of cyan and yellow spheres. The cyan spheres represent water molecules, and the yellow spheres represent polymer ester B molecules. The distribution appears more uniform than in the A hydrate snapshot.

Figure 2. Microscopic observations of hydrates (top) and molecular simulation snapshots of hydrates containing 30% water (bottom).

4.2 Differences in the Presence of Free and Bound Water in Hydrates

We further hypothesized that the differences in water-holding capabilities between Esters A and B are influenced by the strength of interactions between the polymer esters and water. Water is generally classified into three states—free, bound, and non-freezing water—which can be differentiated using DSC [19-21]. To assess water states in the hydrates, DSC analysis was performed. The thermal behavior during cooling and enthalpy changes for Esters A and B, including their pure forms, water alone, and hydrates containing 10% and 30% water, are shown in Figure 3 and Table 2.

Pure Esters A and B displayed broad peaks from -30°C to -10°C, likely due to polymer solidification. For pure water, a large exothermic peak appeared around -15°C (enthalpy change during freezing $\Delta H = -345 \pm 7.2 \text{ J g}^{-1}$). Ester A's 10% hydrate demonstrated a single peak around -38°C ($\Delta H = -17.1 \pm 4.5 \text{ J g}^{-1}$), and the 30% hydrate displayed two peaks at approximately -38°C and -20°C ($\Delta H = -10.9 \pm 2.7 \text{ J g}^{-1}$ and $-66.6 \pm 4.1 \text{ J g}^{-1}$, respectively). In contrast, Ester B's hydrates (10% and 30%) showed only one peak around -20°C ($\Delta H = -15.0 \pm 0.13 \text{ J g}^{-1}$ and $\Delta H = -78.6 \pm 2.7 \text{ J g}^{-1}$, respectively). The large exothermic peak observed around -20°C in the hydrates of Ester A (30% water) and Ester B (10% and 30% water) is attributed to free water, while the smaller exothermic peak at -38°C, present only in Ester A, suggest bound water [19-21]. These findings indicate that Ester A initially binds water as bound

water and, beyond a certain threshold, begins to hold free water—suggesting a mechanism of bulk-free water retention mediated by bound water [22]. Ester B, however, appears to hold water directly as free water, likely by alignment at the interface.

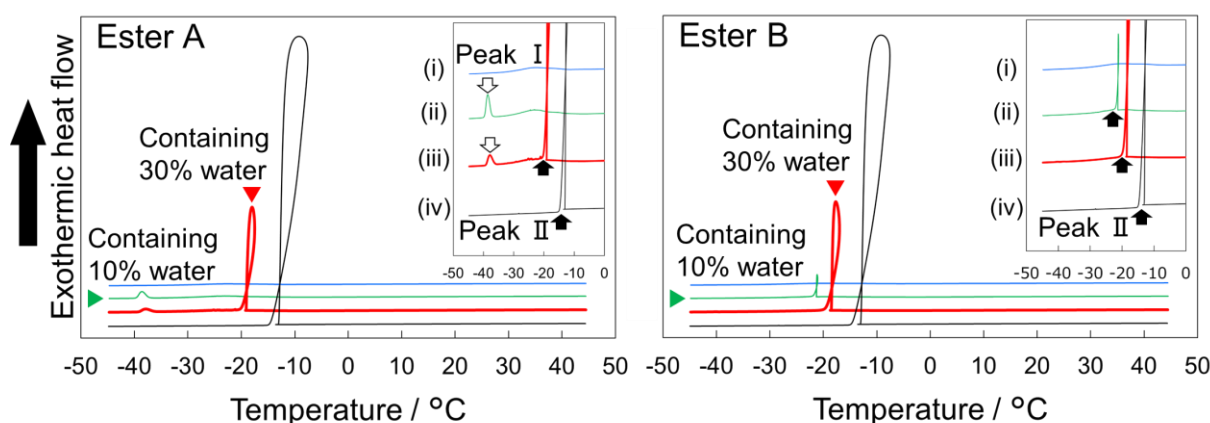


Figure 3. Freezing DSC thermograms of Esters A and B. (i) Pure esters; (ii) hydrates containing 10% water; (iii) hydrates containing 30% water; and (iv) pure water.

Table 2. Enthalpy changes during freezing of hydrates and water as recorded by DSC.

Water content %	Peak I		Peak II		
	$T_{\max}^a / ^\circ\text{C}$	$\Delta H^b / \text{J g}^{-1}$	$T_{\max}^a / ^\circ\text{C}$	$\Delta H^b / \text{J g}^{-1}$	
Ester A	10	-38.5 ± 0.1	-17.1 ± 4.5	N/A ^c	N/A ^c
	30	-37.8 ± 0.1	-10.9 ± 2.7	-18.0 ± 0.0	-66.6 ± 4.1
Ester B	10	N/A ^c	N/A ^c	-20.9 ± 0.4	-15.0 ± 0.1
	30	-39.2 ± 1.3	-0.4 ± 0.0	-17.6 ± 0.2	-78.6 ± 2.7
Water only	100	N/A ^c	N/A ^c	-10.6 ± 3.5	-345.2 ± 7.2

^a Temperature at the peak maximum of the calorimetric exotherm. ^b Enthalpy change associated with freezing. ^c No exothermic peak was observed.

TD-NMR was also used to evaluate the presence of free and bound water [23, 24]. Figure 4 illustrates the T2 relaxation curves of the pure esters and their hydrates. Pure Ester A relaxed slightly faster than Ester B, but both esters were almost fully relaxed by 100 ms. This slight difference was attributed to the disparity in the weight-average molecular weight of the esters. For 10% hydrates, Ester A relaxed more quickly at first, but Ester B surpassed it after 50 ms. A similar trend was observed in the 30% hydrates, with crossover occurring at ~120 ms. Bound water is known to have shorter relaxation times than free water [23, 24], supporting the presence of bound water in Ester A hydrates. In contrast, optical microscopy observations indicated that the water droplets in the Ester B hydrates were smaller than those in Ester A. It is generally accepted in TD-NMR that smaller water droplets lead to a larger oil-water interfacial area, which in turn results in shorter relaxation times [25]. The smaller droplet size in Ester B, confirmed via optical microscopy, increases the oil-water interface, explaining its faster relaxation in later stages.

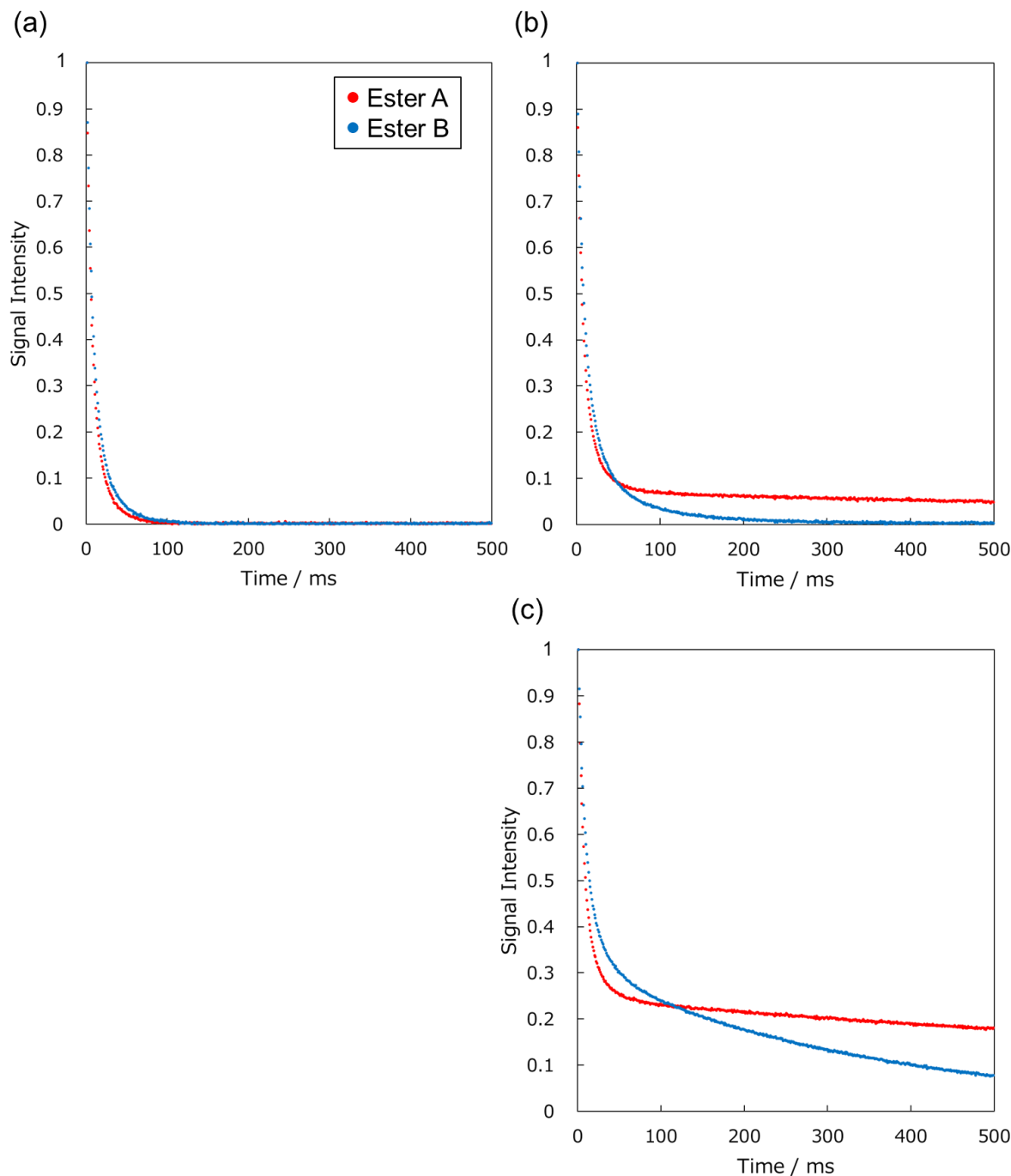


Figure 4. Maximum normalized ¹H TD-NMR relaxation decays. (a) Pure esters; (b) hydrates containing 10% water; and (c) hydrates containing 30% water.

4.3 Impact of Polymer Ester Molecular Structure on Water-Holding Capability

Following observations from optical microscopy (Section 4.1), we hypothesized that the hydrate microstructures of Esters A and B differ. SWAXS analysis was conducted on pure esters and their hydrates with 0.1, 0.5, 1, and 5 g of water per 10 g of ester (Figure 5). In the small-angle region, no peak was observed for Ester A. However, a broad peak around $q = 0.8\text{--}1.0 \text{ nm}^{-1}$ appeared for Ester B, suggesting the formation of reverse micelle-like structures [26]. Given Ester B's low interfacial tension (Section 3.1), it likely functions as a surfactant. In the wide-angle region, both esters showed a peak near $q = 15 \text{ nm}^{-1}$, likely due to ester in a liquid

state [27]. These results imply that Ester A holds water via a different mechanism than Ester B, which holds water by acting as a surfactant.

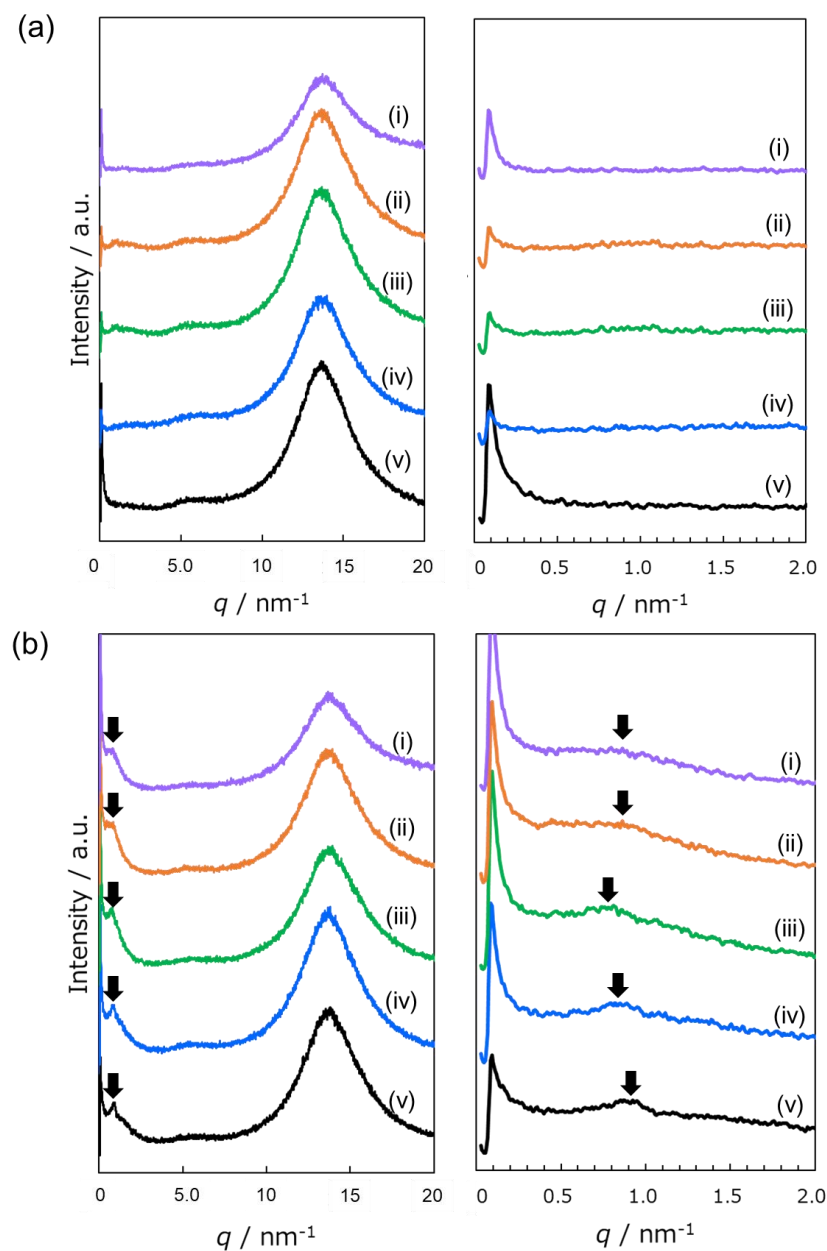


Figure 5. SAXS and WAXS curves of Esters (a) A and (b) B. The ester-to-water ratios are: (i) 10:5, (ii) 10:1, (iii) 10:0.5, (iv) 10:0.1, and (v) 10:0, respectively.

To further investigate the coexistence of water and polymer, DPD simulations were conducted. The end-to-end distances between the terminal hydroxyl (OH) groups of each polymer ester molecule were analyzed. The probability distribution of the end-to-end distance is illustrated in Fig. 6. The curve for Ester A (30% water) exhibits two distinct peaks, whereas that for Ester B (30% water) shows only a single peak. In the case of the two peaks, the connection states between the droplets and the terminal OH groups of the polymer esters are illustrated in Fig. 6(b) and 6(c). As illustrated in Fig. 6(b), both the terminal and central hydrophilic segments of the polymer esters aggregate around one droplet, contributing to the stabilization of the interface by modulating surface tension. Figure 6(c) illustrates a case in which one polymer

ester molecule links two different droplets. After bridging multiple droplets, the central segment of the polymer ester also carried a hydrophilic group, allowing additional water molecules to wet the region between the droplets. This leads to an increased hydrophilicity and water-holding capability of the system as a whole. In contrast, for Ester B, only one peak was observed. Owing to the limited polymer chain length, it is more challenging to bridge two droplets, and polymer esters tend to aggregate on the surfaces of individual droplets. Even if two droplets are linked, the central hydrophilic segment tends to attach to one of the droplets because of its short chain length, thereby reducing the probability of forming water pathways between the droplets. The increased chain length with a higher degree of polymerization enhances the bridging of water molecules and provides more space for water molecules to reside, which may explain why higher polymerization holds bulk water and leads to better water-holding capability.

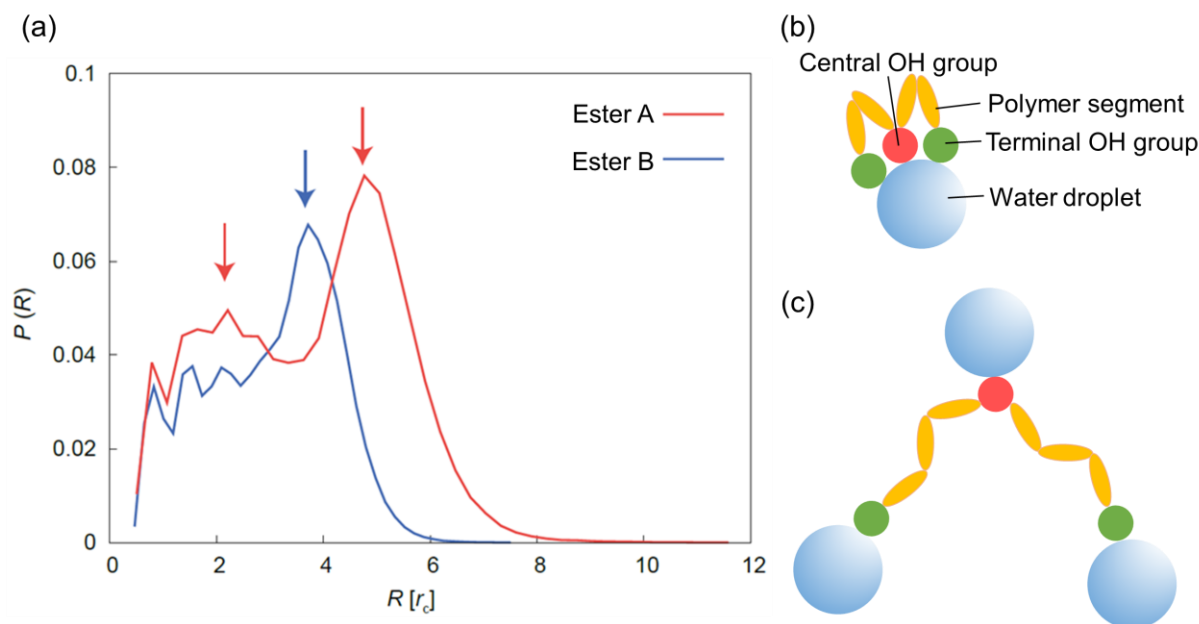


Figure 6. (a) Probability distribution of the distance between terminal OH groups at varying degrees of polymerization; (b) image showing the aggregation of terminal OH groups at the same droplet; (c) image showing the aggregation of terminal OH groups at different droplets.

5. Conclusion

This study investigated Polyglyceryl-2 Dipolyhydroxystearate, a W/O emulsifier, focusing on the relationship between its degree of polymerization and its water-holding capability. The results revealed that Esters A and B exhibit markedly different water-holding behaviors. Ester A demonstrated a high water-holding capability, attributed to its ability to interact with free water via bound water. Its longer polymer chains likely contribute to the formation of a stable water-holding structure through bridging interactions between water droplets. In contrast, Ester B acted primarily as a surfactant, stabilizing water through the emulsification of free water without the involvement of bound water. The absence of polymer chain bridging in Ester B, along with its weaker interaction with water, is considered the primary reason for its lower water-holding capability. These findings clarify the molecular mechanisms by which the degree of polymerization influences water-holding behavior and performance. By integrating experimental approaches with molecular simulations, this study offers a foundation for the design of novel materials with enhanced moisturizing properties. Continued exploration of water-holding mechanisms is expected to support the development of next-generation materials with improved hydration performance.

6. References

1. D. J. Miller et al. *Colloids and Surfaces A: Physicochemical and Engineering Aspects*, 2001, 681-688.
2. D. Venkataramani et al. *Advances in Colloid and Interface Science*, 2020, 102234.
3. S. Ghosh, D. Rousseau. *Current Opinion in Colloid & Interface Science*, 2011, 16, 421-431.
4. A. L. Márquez et al. *Journal of Colloid and Interface Science*, 2010, 341, 101-108.
5. C. W. Pouton. *International Journal of Pharmaceutics*, 1985, 27, 335-348.
6. A. Nesterenko et al. *Colloids and Surfaces A: Physicochemical and Engineering Aspects*, 2014, 457, 49-57.
7. S. Alam et al. *Cosmetics*, 2020, 7, 43.
8. T. Rode et al. *European Journal of Pharmaceutics and Biopharmaceutics*, 2003, 55, 191-198.
9. S. Duprat-de-Paule et al. *Oilseeds and fats, Crops and Lipids*, 2018, 25, D503.
10. H. Paula et al. *American Journal of Infection Control*, 2017, 45, 835-838.
11. T. Goloub and R. J. Pugh. *Journal of Colloid and Interface Science*, 2003, 257, 337-343.
12. R. Pichot et al. *Journal of Colloid and Interface Science*, 2010, 352, 128-135.
13. S. Liu and S. P. Armes. *Current Opinion in Colloid & Interface Science*, 2001, 6, 249-256.
14. D. Vasiljevic et al. *International Journal of Pharmaceutics*, 2006, 309, 171-177.
15. R. D. Groot and P. Warren. *Journal of Chemical Physics*, 1997, 107, 4423-4435.
16. P. B. Warren. *Current Opinion in Colloid & Interface Science*, 1998, 3, 620-624.
17. P. J. Hoogerbrugge and J. M. V. A. Koelman. *Europhysics Letters*, 1992, 19, 155-160
18. P. Espa  ol and P. Warren. *Europhysics Letters*, 1995, 30, 191-196.
19. M. Tanaka et al. *Bull. Chemical Society of Japan*, 2019, 92, 2043-2057.
20. S. M. Dron and M. Paulis. *Polymers*, 2020, 12, 2500.
21. T. Hatakeyama et al. *Thermochimica Acta*, 1988, 123, 153-161.
22. H. Hatakeyama and T. Hatakeyama. *Thermochimica Acta*, 1988, 308, 3-22.
23. C. L. Cooper et al. *Soft Matter*, 2013, 9, 7211-7228.
24. M. C. Vachier and D. N. Rutledge. *Food Chemistry*, 1996, 57, 287-293.
25. P. J. Davis et al. *Powder Technology*, 1987, 53, 39-47.
26. K. Aramaki et al. *Langmuir*, 2015, 31, 10664-10671.
27. S. Kotani et al. *Langmuir*, 2017, 33, 12171-12179.